Available online at www.sciencedirect.com
SCIENCE DIRECT®
Earth and Planetary Science Letters 218 (2004) 197–213
EPSL
www.elsevier.com/locate/epsl

Directions and intensities of the Earth's magnetic field during a reversal: results from the Permo-Triassic Siberian trap basalts, Russia

Christoph Heunemann [a,*], David Krása [a], Heinrich C. Soffel [a], Evguenij Gurevitch [b], Valerian Bachtadse [a]

[a] *Department of Earth and Environmental Sciences, Geophysics Section, Ludwig-Maximilians-Universität München, Theresienstr. 41, 80333 Munich, Germany*

[b] *VNIGRI, Laboratory of Palaeomagnetism, Liteiny Avenue 39, 191104 St. Petersburg, Russia*

Received 22 April 2003; received in revised form 20 October 2003; accepted 21 October 2003

Abstract

An extensive palaeomagnetic study was carried out on an approximately 250 Ma old reversed to normal transition of the Earth's magnetic field (EMF) recorded in 86 volcanic lava flows of the Siberian trap basalts, North Siberia, Russia. In addition to the investigation of the directional behaviour of the field (≈700 specimens) a total of 298 specimens was subjected to Thellier-type palaeointensity determinations. Adding several modifications to the original Thellier experiment, such as tests for MD tails and the additivity of partial thermoremanent magnetisation yields highly reliable palaeointensity estimates of the Late Permian/Early Triassic EMF. Transitional directions of the EMF were obtained from 20 flows. During the reversal a clustering of the virtual geomagnetic poles (VGPs) is observed (15 flows). Palaeointensity estimates suggest that this feature is not an artifact due to rapid flow emplacement since the directional cluster is associated with a well-defined increase in palaeointensity from 6 to 13 μT. Subsequently, the next VGPs move towards the pole position of normal polarity. Departing in a sudden movement from normal polarity the VGPs form a second directional cluster comprising the results of 14 flows. This feature is interpreted as a post-transitional excursion but lacks the characteristic intensity variation recorded during the first transitional cluster. The rest of the section (41 flows) is of normal polarity. The characteristic features of this reversal, low intensities and directional clustering during the reversal and an excursion shortly after the reversal, were also observed in records of polarity transitions of younger age. This suggests that the underlying reversal processes were similar. The mean virtual dipole moment calculated for the stable normal part of the studied section yields a rather low value of $2.2 \pm 0.9 \times 10^{22}$ Am^2. These findings confirm that the Mesozoic Dipole Low extends at least down to the Late Permian/Early Triassic. The geomagnetic VGP dispersion was calculated for the stable normal part of the section and yields values similar to those for the last 5 Ma. Considering that the intensity of the EMF was considerably higher in this time interval than in the Early Triassic, a direct relationship between intensity and secular variation seems unlikely.

* Corresponding author. *E-mail address:* heunem@geophysik.uni-muenchen.de (C. Heunemann).

0012-821X/03/$ – see front matter © 2003 Elsevier B.V. All rights reserved.
doi:10.1016/S0012-821X(03)00642-3

Keywords: palaeomagnetism; absolute palaeointensity; Siberian trap basalts; Permo-Triassic boundary; Mesozoic Dipole Low; reversal mechanism

1. Introduction

In order to understand the processes in the liquid outer core of the Earth where the Earth's magnetic field (EMF) is generated, reliable records of its variations throughout the geological history are essential. Especially data on directional and intensity variations of the transitional field during reversals of the EMF provide important constraints for geodynamo models [1,2]. Although there are numerous studies dealing with the directional behaviour of the field as a function of time, far fewer data on variations of the intensity of the field have been published so far. The limited data set available indicates that the strength of the EMF is strongly reduced during polarity transitions when compared to stable normal or reversed polarities (e.g. [3]). However, these results have been obtained from relatively young rocks. No reliable absolute palaeointensity records of polarity transitions prior to the Cenozoic have been brought forward yet.

The behaviour of the EMF during the Mesozoic and Late Paleozoic, or more precisely between 86 and 276.5 Ma [4], is of particular interest. Its virtual dipole moment (VDM) seems to have been significantly reduced ($\approx 4\times10^{22}$ Am^2, [4]) compared to today's values. This feature, known as the Mesozoic Dipole Low (MDL), was first identified by Bol'shakov and Solodovnikov [5] and Prévot et al. [6] and later confirmed by Tanaka et al. [7] and Perrin and Shcherbakov [8]. In this context detailed studies of polarity reversals can provide valuable information on the underlying processes by comparing transitional patterns observed in Cenozoic reversals with detailed reversal records during the MDL.

Studies of volcanic sequences suggest that rapid changes of the local field direction and directional clustering are characteristic features of reversals (e.g. [9–13]). But as already mentioned the data set needs to be extended substantially in order to prove or disprove the current models about reversal processes.

In this paper we present the results of a palaeomagnetic study of 86 individual flows exposed in three sections of the Permo-Triassic (about 250 Ma) Siberian trap basalts, North Siberia, Russia. The short duration of the volcanic activity and the extremely high lava productivity makes the Siberian trap basalts an excellent object for deciphering the fine structure of the EMF with high temporal resolution. Absolute palaeointensity determinations using the Thellier–Thellier method [14], with several modifications (e.g. [15–20]) further enhancing the reliability of the results, were performed in order to assess information on the intensity variation before, during and after the reversal. The stratigraphically lower section contains three successive flows of reversed polarity followed by flows which recorded a transitional state of the EMF. The upper section shows normal polarity and a group of directions which is tentatively interpreted as an excursion. These palaeodirectional results are described in detail in Gurevitch et al. [21]. Additional data from boreholes in that study, penetrating the complete lava pile in the Noril'sk region, prove that this reversal is the only one which occurred during the emplacement of the Noril'sk traps. Directional data presented here are based on a slightly different data set with less flows sampled but with more individual samples per site, thus displaying small deviations compared to the above-mentioned study [21]. The resulting mean pole positions, however, of the two studies are almost identical (56.2°N/146.0°E study [21], 57.1°N/148.2°E this study, see Table 1).

2. Geology and sampling

Siberian Trap volcanism produced a huge pile of basaltic flows deposited in the Tunguska Syncline of the Siberian platform and on Gorny Taimyr and represents the largest terrestrial continental igneous province (Fig. 1a, shaded areas). The extrusive rocks cover today an area of 3.4×10^5

Table 1
Calculated mean poles for the individual directional groups of the Listvjanka and Icon/Abagalakh sections (see text)

Group	N	Dec	Inc	k	α_{95}	VGP		d_p/d_m	Comment
		(°)	(°)	(°)		Longitude (°)	Latitude (°)	(°/°)	
D	41	88.5	75.4	77.9	2.5	148.2 (6.6)	57.1 (85.1)	4.3/4.7	N (ND5–KMX4)
C	14	21.9	68.4	233.3	2.6	230.4 (297.9)	68.7 (52.6)	3.7/4.4	E (TK5–ND6)
B	15	151.4	54.0	337	2.2	114.3 (98.5)	16.6 (42.1)	2.2/3.1	T (SV1–GD1, TA6–TA8)
A	5	250.9	−68.1	106	8.4	7.1 (76.7)	−53.7 (−69.7)	12/14	R (IV2–IV4, TA3–TA4)
		87	76	81	5.1	144	60	–/–	Lind et al. [32]

For each group the number of sites (N), the mean declination (Dec) and inclination (Inc) with their respective 95% confidence cones (α_{95}) and precision parameter k are shown. Also given the associated VGP positions (latitude/longitude) and the parameters of the confidence oval (in parentheses: VGP position after correction for plate motion). N: normal, E: excursion, T: transitional, R: reversed. For comparison results of Lind et al. [32] are included in the table (average of all suites, reversed polarity inverted).

km^2 and the original volume of this igneous province was probably considerably greater than 2×10^5 km^3 [22]. Recent results of Reichow et al. [23] show that the volcanic province extends far into the West Siberian Basin, where the basalts are covered by Mesozoic and Cenozoic sediments, thus increasing the area of the province even more. The composite sequence of the volcanic province sums up to a thickness of 6.5 km. Precise U–Pb zircon and baddeleyite ages (251.2 ± 0.3 Ma, [24]) and ^{40}Ar–^{39}Ar data (250.0 ± 1.6 Ma, [25]) place the onset of the volcanic activity, within margin of error, at the Permo-Triassic boundary (for an overview of published ages see also [23]). Geological evidence and radiometric ages suggest that the traps erupted in an extremely short time interval of only 0.9 ± 0.8 Ma [26]. Given the size and the simultaneity of this volcanic activity it is very likely that this event contributed to the greatest extinction of flora and fauna in Earth's history, the Permo-Triassic crisis (e.g. [27,28]).

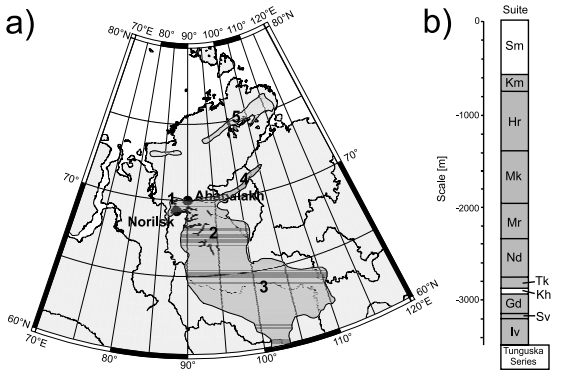

Fig. 1. (a) North Central Siberia, Russia. Grey shaded areas indicate the Permo-Triassic Siberian trap basalts. Numbers indicate the regional subdivision of the traps: (1) Noril'sk, (2) Putorana, (3) Nizhnaya-Tunguska, (4) Maimecha-Kotuy and (5) Taimyr. (b) Composite stratigraphy of the Siberian trap basalts in the Noril'sk area (modified after Lind et al. [32]). Given also the approximate thickness of the individual suites (Iv, Ivakinsky; Sv, Syverminsky; Gd, Gudchikhinsky; Kh, Khakanchansky; Tk, Tuklonsky; Nd, Nadezhdinsky; Mr, Morongovsky; Mk, Mokulaevsky; Hr, Kharaelakhsky; Km, Kumginsky; Sm, Samoedsky). Sampled suites are marked by grey shading.

The emplacement mechanisms and the magma sources are still heavily debated. There is close temporal correlation between phases of (aborted) rifting at the western boundary of the traps and the volcanic activity. Courtillot et al. [29] suggested that rifting was triggered by an upwelling mantle plume. Nikishin et al. [30], however, argue for a preexisting rift system which was then penetrated by a plume in the Late Permian.

The volcanic province is generally subdivided into five distinct geographic regions: (1) Noril'sk, (2) Putorana, (3) Nizhnaya-Tunguska, (4) Maimecha-Kotuy and (5) Taimyr (Fig. 1a). The flood basalts in the Noril'sk area represent a particularly thick sequence (3.5 km, [22]) with a high ratio of lavas to tuffs. No significant interbedded sedimentary rocks or palaeosols are present in the whole trap basalt sequence. Due to the occurrence of rich Cu–Ni sulfide deposits in the Noril'sk region, the volcanic sequence was studied exten-

sively because of its economical importance and good geochemical data are available. Lavas of the Noril'sk sequence vary in composition from trachybasalts and basaltic andesites to picritic basalts. A total of 11 suites (Fig. 1b) has been defined on the basis of their chemical composition and texture of the lavas (e.g. [31,32]). The lower part of the Siberian trap basalt province is nowhere else exposed with such a high resolution.

The sections studied are located in the Listvjanka (69°28′N, 88°43′E) and Icon/Abagalakh river valleys (70°22′N, 90°04′E). The Listvjanka section, sampled in summer 2001, is located approximately 9 km east of Talnakh, a small town in the vicinity of Noril'sk. It comprises the Ivakinsky suite (the oldest suite of the Siberian flood volcanism in the Noril'sk area overlying directly the Late Permian sediments of the Tunguska series) up to the Gudchikhinsky suite, totaling 20 consecutive flows. Outcrops along the Listvjanka river are of excellent quality and samples were taken in the lower part of the flows. A parallel profile of seven flows (Talnakh section, Ivakinsky and lowermost part of the Syverminsky suite) was sampled in 2000. The Abagalakh and its directly adjoining downward continuation, the Icon section, both about 130 km NE of Noril'sk, were sampled in summer 2000 and 2001. The outcrops represent the northern rim of the Putorana Plateau. Here, a total of 59 flows was sampled from the Tuklonsky to the top of the Kumginsky suite. The composite section covers practically the whole pile of volcanics in the Noril'sk area. Minor stratigraphical gaps (some tens of metres) are present in the Abagalakh section. The only major stratigraphical gap (max. 130 m) comprises the Khakanchansky suite which was not present in the Listvjanka or the Icon/Abagalakh sections.

The lava flows are mainly tholeiitic or alkaline to subalkaline basalts with a thickness ranging from 3 to 45 m. Intercalated tuff layers could not be sampled due to the bad quality of these outcrops. Stratigraphic position, thickness and bedding of the flows was determined by using borehole data and aerial photographs or directly in the field. At least six samples were taken in the middle or lower part of each flow with a gasoline driven drilling machine. The cores were oriented in the field using a magnetic and, whenever possible, a Sun compass.

3. Palaeointensity determination

3.1. Sample selection and rock-magnetic investigations

The first step in selecting samples for the palaeointensity experiments was to analyse their natural remanent magnetisation (NRM) demagnetisation behaviour. Almost all specimens are dominated by a single stable component, except in few cases where a weak secondary overprint, removed at $\approx$350°C, could be observed (see also [21]). Sites with inconsistent palaeomagnetic results (TA1-2, IV4, HR8, KM4) were excluded. Determinations of the viscosity index [9] for the flows investigated yielded generally values below 5%.

Examination of polished sections from all flows sampled show magnetite/ilmenite intergrowths (exsolution lamellae) in most cases (Fig. 2). This feature is a clear indication for primary high-temperature oxidation. It occurs deuterically during cooling of subaerial basalts between 900 and 500°C [33]. Additional electron microscopical observations and energy dispersive X-ray (EDX) analysis confirm this interpretation qualitatively on the basis of the Fe/Ti ratios of the two different phases. Thus, the measured palaeodirectional and intensity information obtained from these flows was acquired during or shortly after extrusion of the basalts.

At least one specimen from each flow was subjected to rock-magnetic investigations using a variable field translation balance (VFTB). Strong field thermomagnetic curves are in most cases reversible. The dominant minerals are magnetite as well as Ti-poor titanomagnetite with Curie temperatures (T_C) between 530 and 590°C. A few samples exhibit relatively low T_C down to 440°C which corresponds to a titanium content $x \simeq 0.2$ [33]. 10 samples have two T_C, usually one close to the Curie temperature of magnetite, the other one around 500°C.

For a subset of 24 flows, continuous demagnet-

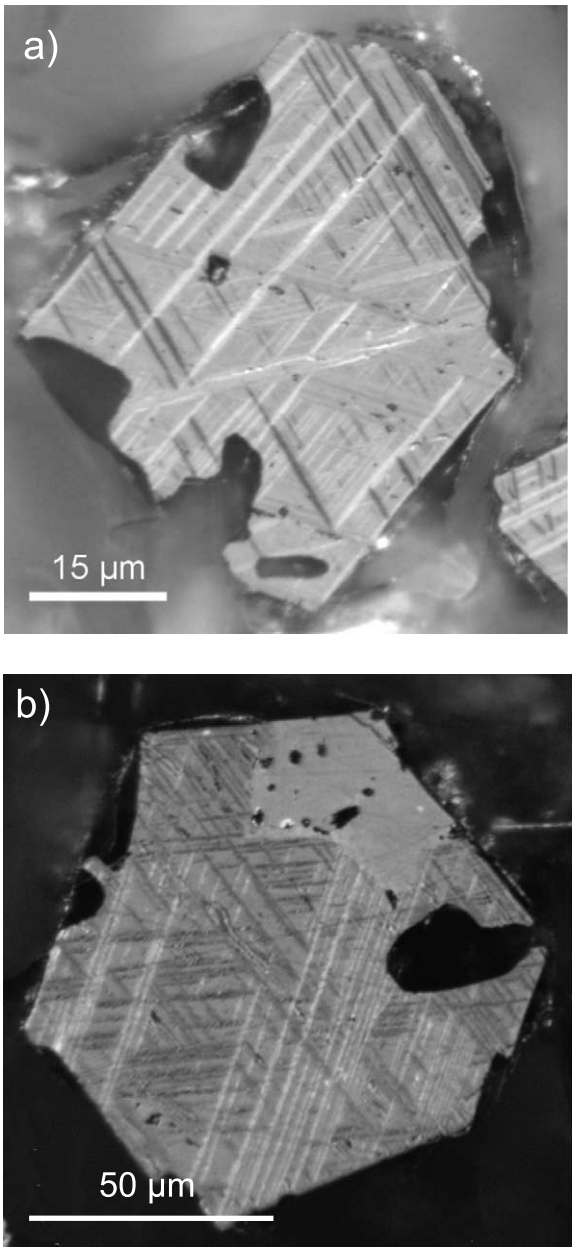

Fig. 2. Photomicrographs of polished sections under crossed Nicols (a: sample HR2-3, b: sample KMX1-3). Optically anisotropic ilmenite/(titano-)magnetite exsolution lamellae are clear evidence for high-temperature oxidation of titanomagnetite.

isation curves were measured with a high-temperature spinner magnetometer (HOTSPIN, [34]). Samples were heated successively to maximum temperatures of 100, 200, 350, 500 and 600°C to test for self-reversal or partial self-reversal. The data indicate that the largest part of the primary remanence unblocks close to T_C, which proves that the carriers of the remanence are indeed magnetite and low-Ti titanomagnetites. In one case (flow KM4) self-reversal could be identified during HOTSPIN measurements.

Two sites (SV8 and SV9) have anomalously high Curie temperatures and carry remanences with maximum blocking temperatures of up to 640°C or even 670°C. In addition to magnetite these samples also contain a hematite component which is clearly visible in the decay plot of the NRM versus demagnetisation temperature. Both components carry identical directions. Polished sections reveal tiny reddish hematite grains arranged around larger (titano-)magnetite grains.

3.2. Methods of the palaeointensity experiments

A modified Thellier–Thellier technique [14] was used to determine absolute palaeointensities. These modifications with partial thermoremanent magnetisation (pTRM) [15] and tail checks (MD checks) are described in [16–19]. At every second heating step a pTRM check (CK) was performed in order to monitor alteration processes continuously throughout the experiment. At some temperatures (e.g. 200, 380, 480 and 520°C) the pTRM was again demagnetised in zero field up to the same temperature as the pTRM acquisition ($NRM_{re}(T_i)$). The remanences after the first demagnetisation step ($NRM(T_i)$) and after the repeated demagnetisation are compared. Differences between the two measurements may have two causes which both severely bias the result of the experiment: (1) Changes in direction between $NRM(T_i)$ and $NRM_{re}(T_i)$ are interpreted as evidence for alteration products with higher blocking temperatures. (2) Significant differences in intensity without directional deviations are an indication of MD particles dominating the magnetic properties of the specimens [16].

Beyond this, most of the specimens were sub-

jected to additivity checks (AC). These checks are described in Krása et al. [20] and consist basically of an additional demagnetisation step (up to a temperature T_2) after a pTRM acquisition (pTRM(T_1, T_0), with $T_2 < T_1$ and T_0 denoting room temperature). If the law of additivity is fulfilled, a prerequisite essential for a reliable palaeointensity estimate, the remaining magnetisation should equal the difference pTRM(T_1, T_0)−pTRM(T_2, T_0).

A total of 298 samples was subjected to the experiments described above. Most samples have a diameter and length of 5 mm ('mini'-specimens). 40 samples with a diameter/length of 9 mm were used. All these daughter specimens were obtained from the lower part of standard inch-sized specimens and not oriented with respect to the original core. To ensure the primary character of the magnetisation the mother specimen (inch core) was stepwise thermally demagnetised and its demagnetisation behaviour compared to that of the respective daughter specimen of the same drill core. Only 'mini'-specimens showing similar behaviour as the inch specimens were analysed with respect to their palaeointensity information. All samples were heated in a MMTD20 thermal demagnetiser and measured with a 2G cryogenic magnetometer located in a shielded room. The applied field intensity during pTRM acquisition ranged between 18 and 35 μT. 45 specimens were heated and cooled in a quartz-glass tube in an inert argon atmosphere, all others in air. Results for all accepted palaeointensity determinations are independent of the sample size, applied field intensity or the atmosphere to which the samples were exposed during heating and cooling.

3.3. Reliability criteria

The data were analysed using NRM–TRM (Arai) plots [35]. The criteria listed below were used to assess the quality of the experimental palaeointensity data:

1. In order to ensure that the magnetisation is of primary origin the temperature range of the linear fit has to match the temperature range of the characteristic remanent magnetisation of the respective inch sample. The maximum mean angular deviation in this interval must not exceed 5°.
2. A minimum of five consecutive data points is required for a linear fit.
3. Less than 10% standard deviation of the linear fit.
4. At least 30% of the NRM (fraction f) has to be covered by the linear fit.
5. The difference between pTRM check and pTRM acquisition (CK error), normalised to the total TRM, has to be less than 5% before and within the linear segment to ensure that the effect of chemical alteration does not bias the results.
6. Within the linear segment, the remanence of the NRM in core coordinates or after a MD tail check should not move towards the direction of the applied field.
7. The limit for a successful MD tail check is 10% ($|\mathrm{NRM}(T_i) - \mathrm{NRM}_{re}(T_i)| < 0.1$) and the difference in direction should not exceed 9°.
8. As proposed by Krása et al. [20] the threshold for an acceptable AC error is 7% (normalised to the total TRM). This criterion could be applied only to 50% of the samples.

If conditions (1)–(7) are fulfilled, the result is classified as class A determination (63 samples). Violation of criteria (1) or (2) leads to immediate rejection. If only one of the other criteria is not fulfilled the result is a class B determination (80 samples). The upper limits for a B result are: standard deviation of the linear fit $< 15\%$, $20\% < f < 30\%$, CK error $< 7\%$, MD checks $< 15\%$, $\sphericalangle(\mathrm{NRM}(T_i), \mathrm{NRM}_{re}(T_i)) < 15°$ and AC $< 10\%$. All other results were rejected.

3.4. Interpretation of the NRM–TRM plots

Representative examples for palaeointensity determinations and their associated Zijderveld plots ([36], in core coordinates) of the two quality classes are shown in Fig. 3. Fig. 4 depicts some rejected results. In most cases of rejected results, alteration caused the destruction or formation of remanence carrying material in the course of the experiment (Fig. 4a). Some samples show a clear concave curvature of the NRM–TRM plot which is indicative for the dominating role of MD par-

ticles. The presence of this MD tail gives estimates of the palaeointensity in the high temperature range which are systematically too low and were therefore excluded from further interpretation. In the lower temperature range the direction of the remanence does not resemble the primary component of the magnetisation (Fig. 4b), as could be shown for the respective sister specimens (inch cores). These specimens were also rejected.

Reliable palaeointensity estimates were obtained for ≈50% of the samples (Table 2). Fig. 5a–f show representative results of the experiments for different stratigraphic levels. If a certain fraction of thermally demagnetised samples from one flow shows an overprint, the interpretation of

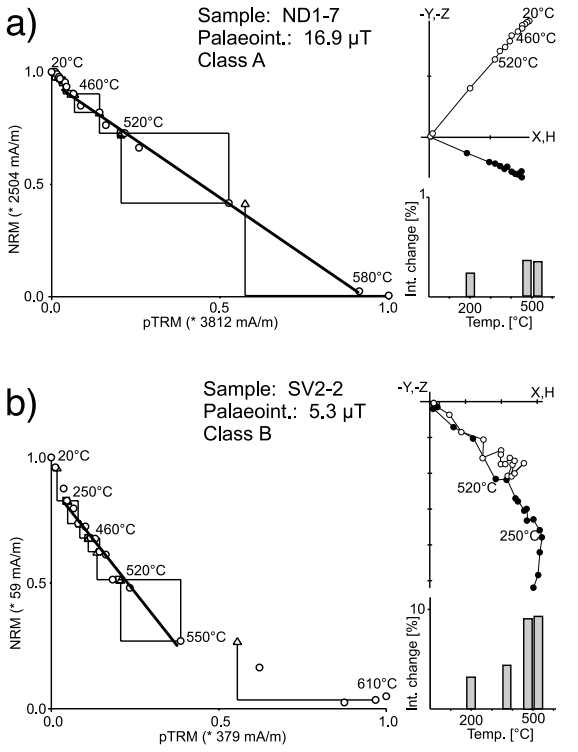

Fig. 3. Representative examples for (a) class A and (b) class B palaeointensity determinations. Open symbols in the Zijderveld plots [36] correspond to the projection onto the vertical plane, solid symbols onto the horizontal plane. The linear segment covers the same temperature range as the characteristic remanent magnetisation (all Zijderveld plots are in core coordinates). Results of the pTRM and AC checks are indicated by triangles (horizontal and vertical lines below the data points) and squares (horizontal and vertical lines above the data points), respectively.

all NRM–TRM plots of samples from this flow was restricted to the temperature range above the maximum unblocking temperature of this overprint (like in flows IV2 and TK7). In some cases the MD tail and AC indicate that the remanence in the low blocking temperature (T_b) range is biased by MD behaviour. Regarding the initial drop in NRM in examples Fig. 5e and f we think that it is more plausible that the primary information is carried by the high-temperature slope. It is difficult to conceive that the magnetite, being of primary origin (high-temperature oxidation), carries more reliable information in the low-temperature range which covers only a small fraction of the NRM. Biasing MD contribution can be ruled out in the high-temperature range. Most of the determinations cover a fraction of the NRM between 40 and 80% and have a quality factor q, as defined by Coe et al. [37], of 5–15. The weighted mean palaeointensity was calculated according to Prévot et al. [9]. No reliable palaeointensity estimates were obtained for samples of the Talnakh section.

In the cases of flows SV8 and SV9, a hematite component in addition to magnetite is identified (see also rock-magnetic investigations). The palaeomagnetic direction carried by the hematite is identical to that of the magnetite component. Moreover, when analysing the palaeointensity information carried by magnetite alone and the information carried by both components only minor differences in the results are observed (1–2 µT). This makes two scenarios feasible: (1) The whole flow was reheated above the Curie temperature by the following flow. However, it is rather unlikely that the heat input from above affected the flows (more than 3 m thick) as a whole. Anyway, great care was taken to sample only the lower parts of the flows. (2) The formation of hematite is more or less coeval with the emplacement of the flow which means the magnetisation in both components is primary and was acquired soon after the extrusion of the flows during cooling down to ambient temperatures. However, this alternative is still under investigation. Palaeointensity estimates for the two flows in question were therefore determined solely for the temperature range of the magnetite component.

Fig. 6 shows the declination, inclination, weighted mean palaeointensities (for some flows individual results) and the calculated VDM across the studied sections.

4. Results and discussion

The directional record of the Listvjanka section, as illustrated in Fig. 7, starts with three flows of reversed polarity (group A, Ivakinsky suite). Then, a directional cluster comprising the results of 12 flows is reached (group B, flows SV1 to GD1). These directions are 48° off the pole of stable normal polarity (see below), and were thus classified as transitional. Note that this angle clearly exceeds well the cut-off angle estimated by the analyses of the secular variation discussed in detail below. Results of the parallel Talnakh section show a very similar behaviour, i.e. reversed polarity at the base of the section followed by an intermediate direction and finally reaching the same position (three flows) as the cluster identified in the Listvjanka section (Fig. 7a, open diamonds). The following three flows of the Listvjanka section (flows GD2–GD4) each have a different direction. GD5 reaches normal polarity. After the gap of the Khakanchansky suite two flows of normal polarity are identified. 14 consecutive flows (TK5 to ND6, labelled group C) recorded deviant directions (36° great circle distance) from normal polarity. We interpret this tentatively as an excursion or post-transitional rebound effect (e.g. [38]). Subsequently normal polarity is reached (group D). Comparing these results to palaeomagnetic data for the Siberian platform for the time interval between 248 and 253 Ma shows good agreement (virtual geomagnetic pole (VGP) longitude: 151°N, latitude: 52°E, k: 97, A_{95}: 8.8°; [39]). When correcting the VGPs for the Permo-Triassic palaeogeography (Table 1, corrected VGPs in brackets) the resulting position of group D is, within margin of error of the rotation parameter (0°N, 63°E, +37°; [39]) and the α_{95} of this study, indeed of normal polarity. Groups A and D are nearly antipodal but do not pass a reversal test ([40], observed angular difference: 8.6°; critical angular difference 7.7°).

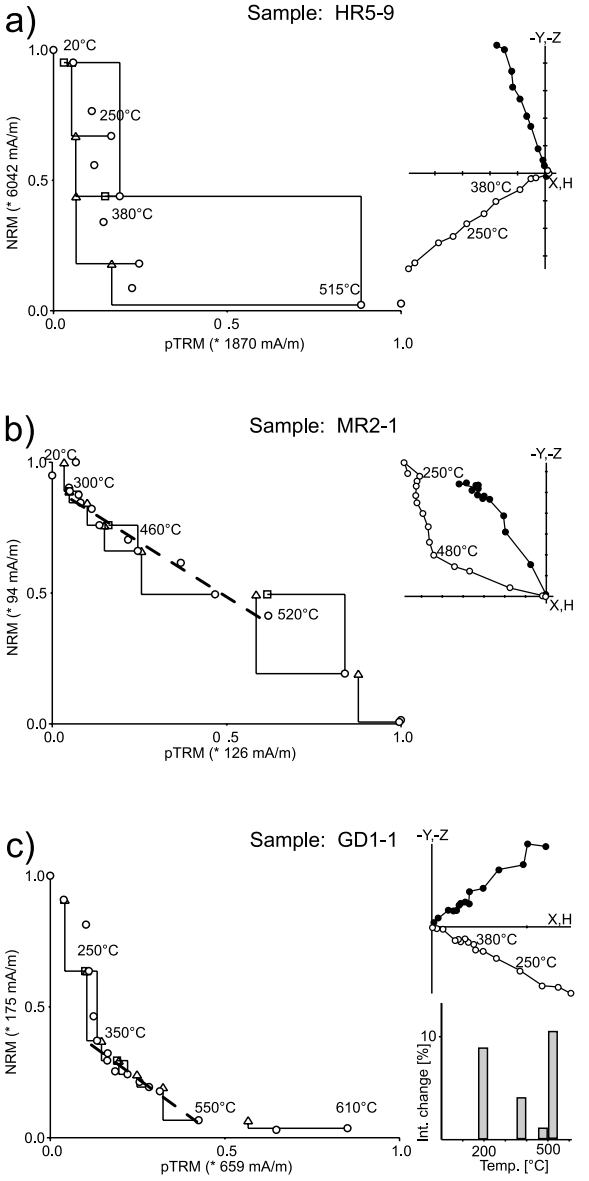

Fig. 4. Typical examples of rejected palaeointensity results due to: (a) alteration, (b) mismatch of temperature range of the characteristic remanent magnetisation and the temperature range of the linear segment. In some cases the reliability criteria are exceeded in several parameters and were thus excluded from further interpretation. (in example (c) pTRM check error > 8%, MD check > 10%).

This can be attributed to the limited number of flows of reversed polarity. Another explanation is that the VGPs of group A are very close to the reversal and already show directions which are

Table 2
Results of the palaeointensity experiments[a]

Site	Dec	Inc	N_d	k	α_{95}	n/N	Sample	Cl.	ΔT	N_p	f	g	q	w	$F_p \pm \sigma_{F_p}$	$\tilde{F}_p \pm \sigma_{\tilde{F}_p}$
Abagalakh section																
KMX4 (km7)	37	77	6	182	5.0	2/4	KMX4-3	B	545–590	5	0.63	0.64	10.9	6.3	38.1 ± 1.4	37.6 ± 1.0
							KMX4-6	B	420–530	5	0.40	0.61	4.8	2.8	36.3 ± 1.9	
KMX3 (km6)	47	74	8	98	5.6	4/4	KMX3-1	B	420–580	7	0.83	0.80	26.1	11.7	32.1 ± 0.8	30.8 ± 2.7
							KMX3-2	B	420–610	8	0.87	0.81	14.3	5.9	36.9 ± 1.8	
							KMX3-3	B	535–590	6	0.46	0.77	14.0	7.0	26.4 ± 0.7	
							KMX3-6	A	300–530	9	0.44	0.69	10.6	4.0	25.4 ± 0.7	
KMX2 (km5)	68	72	8	446	2.6	2/5	KMX2-4	B	250–420	6	0.36	0.75	6.6	3.3	10.9 ± 0.5	12.0 ± 2.2
							KMX2-5	B	250–420	6	0.33	0.73	2.3	1.2	15.0 ± 1.5	
KMX1 (km4)	75	72	7	644	2.4	2/3	KMX1-2	B	360–530	7	0.54	0.61	8.6	3.9	18.6 ± 0.7	22.0 ± 6.1
							KMX1-4	A	390–530	6	0.36	0.67	3.3	1.6	29.9 ± 2.2	
KM4 (km3)																
KM3 (km2)	75	73	7	510	2.7	3/5	KM3-2	B	250–530	10	0.71	0.76	7.3	2.6	11.5 ± 0.9	11.5 ± 1.2
							KM3-4	B	200–530	11	0.69	0.80	10.8	3.6	10.6 ± 0.5	
							KM3-5	B	20–440	9	0.45	0.80	3.19	1.21	14.1 ± 1.6	
KM1 (km1)	69	72	7	273	3.7	2/6	KM1-2	A	250–520	6	0.50	0.58	2.9	1.5	12.4 ± 1.2	16.5 ± 3.6
							KM1-5	A	370–520	6	0.33	0.54	3.7	1.8	19.6 ± 0.9	
HR13 (hr8)	59	81	9	148	4.2	2/4	HR13-1	B	515–590	8	0.78	0.79	19.2	7.9	12.9 ± 0.4	14.8 ± 1.7
							HR13-3	B	450–580	6	0.87	0.69	17.9	9.0	16.4 ± 0.6	
HR11 (hr7)	50	75	8	156	4.4	2/4	HR11-2	A	200–480	9	0.50	0.74	6.2	2.4	14.0 ± 0.8	13.7 ± 0.3
							HR11-6	B	535–590	6	0.22	0.65	5.7	2.9	13.4 ± 0.3	
HR8 (hr6)																
HR7 (hr5)	96	73	8	71	6.6	2/4	HR7-5	B	515–590	8	0.40	0.81	8.1	3.3	32.3 ± 1.3	29.6 ± 2.2
							HR7-6	B	300–530	9	0.64	0.77	16.1	6.1	28.1 ± 0.9	
HR6 (hr4)	109	64	6	1071	2.0	2/4	HR6-1	B	20–610	16	1.00	0.81	23.9	6.4	16.1 ± 0.6	16.8 ± 1.8
							HR6-4	A	420–530	5	0.36	0.65	3.0	1.7	19.2 ± 1.5	
HR5 (hr3)	105	66	7	114	5.8	0/3										
HR3 (hr2)	85	53	9	166	4.0	4/4	HR3-2	A	200–580	13	0.88	0.74	13.7	4.1	14.9 ± 0.7	19.9 ± 2.0
							HR3-3	A	510–610	5	0.81	0.70	12.3	7.1	22.9 ± 1.1	
							HR3-4	A	515–590	8	0.73	0.83	15.2	6.2	22.8 ± 0.9	
							HR3-7	A	20–580	15	0.97	0.81	27.9	7.7	17.6 ± 0.5	
HR2 (hr1)	94	61	8	476	2.5	3/3	HR2-3	A	300–530	9	0.45	0.69	5.2	2.0	13.0 ± 0.8	12.8 ± 0.4
							HR2-4	A	20–610	16	1.00	0.85	18.3	4.9	12.0 ± 0.6	
							HR2-5	A	20–580	15	0.98	0.75	19.1	5.3	13.4 ± 0.5	
MK13 (mk13)	95	71	8	466	2.6	2/3	MK13-6	B	360–530	7	0.64	0.69	5.7	2.5	19.9 ± 1.5	17.7 ± 2.2
							MK13-9	B	360–530	7	0.62	0.68	5.6	2.5	15.5 ± 1.2	
MK12 (mk12)	100	70	8	108	5.5	1/3	MK12-2	B	300–450	6	0.57	0.68	9.4	4.7	11.8 ± 0.5	
MK11 (mk11)	90	76	7	306	3.7	0/3										
MK10 (mk10)	89	66	10	53	6.7	0/5										
MK9 (mk9)	68	67	9	233	3.4	0/4										
MK8 (mk8)	106	79	10	161	3.8	2/5	MK8-6	B	250–420	6	0.36	0.65	2.3	1.2	18.0 ± 1.9	20.5 ± 1.8
							MK8-7	B	420–610	8	0.91	0.78	18.0	7.4	20.9 ± 0.8	
MK7 (mk7)	95	77	7	218	4.1	1/5	MK7-7	A	200–580	13	0.83	0.73	9.4	2.8	21.7 ± 1.4	
MK5 (mk6)	123	82	10	94	5.0	2/5	MK5-3	B	200–420	7	0.81	0.65	5.4	2.4	16.4 ± 1.6	16.4 ± 0.03
							MK5-4	B	200–420	7	0.77	0.68	4.2	1.9	16.4 ± 2.1	
MK4 (mk5)	66	74	8	316	3.1	2/3	MK4-5	B	20–610	16	0.99	0.63	23.2	6.2	16.5 ± 0.5	16.3 ± 0.2
							MK4-6	B	450–610	7	0.95	0.62	16.1	7.2	16.1 ± 0.6	
MK3 (mk4)	84	72	10	455	2.3	3/3	MK3-1	A	330–530	8	0.38	0.73	3.0	1.2	12.0 ± 1.1	10.4 ± 0.8
							MK3-3	A	100–530	12	0.39	0.74	4.5	1.4	10.4 ± 0.7	
							MK3-4	A	360–530	7	0.42	0.65	5.3	2.4	9.5 ± 0.5	
MK2 (mk3)	161	75	9	344	2.8	4/4	MK2-2	B	510–610	5	0.86	0.61	25.7	14.8	14.7 ± 0.3	12.4 ± 1.5
							MK2-4	A	420–580	7	0.92	0.68	8.6	3.9	9.3 ± 0.7	
							MK2-5	A	515–590	8	0.62	0.83	8.2	3.4	9.2 ± 0.6	
							MK2-6	B	390–550	7	0.56	0.63	13.4	6.0	10.4 ± 0.3	

Table 2 (*Continued*).

Site	Dec	Inc	N_d	k	α_{95}	n/N	Sample	Cl.	ΔT	N_p	f	g	q	w	$F_p \pm \sigma_{F_p}$	$\tilde{F}_p \pm \sigma_{F_p}$
MK1 (mk2)	141	78	9	152	4.2	2/4	MK1-1	B	510–610	5	0.83	0.66	7.1	4.1	42.2 ± 3.3	34.6 ± 6.4
							MK1-3	B	420–610	8	0.87	0.83	15.3	6.2	29.6 ± 1.4	
MK0 (mk1)	110	75	10	353	2.6	2/4	MK0-3	B	300–610	12	1.00	0.75	12.4	3.9	21.9 ± 1.3	21.6 ± 0.3
							MK0-5	B	420–580	7	0.96	0.70	7.5	3.3	21.3 ± 1.9	
MR1 (mr11)	117	77	9	512	2.3	4/5	MR1-1	B	330–530	8	0.76	0.78	9.4	3.9	12.7 ± 0.8	13.8 ± 1.1
							MR1-2	B	200–530	11	0.68	0.79	9.3	3.1	14.7 ± 0.9	
							MR1-5	B	330–530	8	0.75	0.77	9.8	4.0	11.8 ± 0.7	
							MR1-6	A	300–550	9	0.79	0.73	9.2	3.5	16.6 ± 1.0	
MR2 (mr10)	115	78	7	285	3.7	1/4	MR2-2	B	360–510	6	0.65	0.76	8.4	4.2	20.4 ± 1.2	
MR4 (mr9)	73	76	8	252	3.6	0/4										
MR6 (mr8)	96	74	7	390	3.1	3/3	MR6-2	A	420–580	7	0.91	0.77	11.4	5.1	20.6 ± 1.3	23.3 ± 1.7
							MR6-3	A	420–530	5	0.42	0.68	5.0	2.9	26.3 ± 1.5	
							MR6-8	A	480–580	5	0.88	0.67	12.7	7.3	23.9 ± 1.1	
MR7 (mr7)	89	77	10	306	2.8	2/3	MR7-2	B	420–530	5	0.63	0.69	8.3	4.8	28.0 ± 1.5	26.4 ± 2.5
							MR7-7	A	390–530	6	0.51	0.73	4.9	2.5	23.3 ± 1.8	
MR9 (mr6)	187	82	7	441	2.9	3/5	MR9-4	B	300–530	9	0.74	0.73	13.0	4.9	20.8 ± 0.9	19.7 ± 0.6
							MR9-5	B	390–530	6	0.70	0.66	8.6	4.3	18.6 ± 1.0	
							MR9-6	A	400–550	6	0.71	0.65	11.4	5.7	19.6 ± 0.8	
MR11 (mr5)	136	81	9	676	2.0	3/5	MR11-3	A	430–550	5	0.68	0.48	74.4	42.9	22.6 ± 0.1	22.5 ± 0.7
							MR11-4	B	390–530	6	0.68	0.63	5.2	2.6	22.0 ± 1.8	
							MR11-8	B	420–580	7	0.90	0.77	7.5	3.4	20.8 ± 1.9	
Icon section																
MR20 (mr4)	98	78	6	1064	2.1	0/4										
MR21 (mr3)	91	80	6	325	3.7	0/4										
MR22 (mr2)	77	77	6	619	2.7	0/3										
MR23 (mr1)	91	77	4	253	5.8	1/3	MR23-1	A	300–610	12	0.92	0.85	18.0	5.7	14.6 ± 0.6	
ND1 (nd1)	100	73	8	1412	1.5	1/4	ND1-7	A	380–580	9	0.94	0.71	28.6	10.8	16.9 ± 0.4	
ND3 (nd3)	40	81	7	802	2.1	0/3										
ND4 (nd4)	72	75	8	156	4.4	2/3	ND4-1	A	440–580	7	0.86	0.71	16.4	7.4	19.3 ± 0.7	19.2 ± 0.3
							ND4-4	A	250–520	10	0.65	0.81	5.9	2.1	18.8 ± 1.7	
ND5 (nd5)	54	72	7	1110	1.8	3/4	ND5-1	B	410–520	6	0.57	0.71	5.9	3.0	6.2 ± 0.4	8.8 ± 2.3
							ND5-3	A	480–580	5	0.80	0.59	10.3	6.0	10.9 ± 0.5	
							ND5-5	A	545–590	5	0.46	0.72	3.8	2.2	6.4 ± 0.6	
ND6 (nd6)	14	69	7	778	2.2	3/3	ND6-1	B	350–580	10	0.90	0.82	9.0	3.2	27.3 ± 2.2	23.3 ± 2.0
							ND6-3	B	440–580	7	0.75	0.74	7.1	3.2	20.7 ± 1.6	
							ND6-7	B	460–580	6	0.75	0.68	14.7	7.3	22.6 ± 0.8	
ND7 (nd7)	4	72	8	611	2.2	4/4	ND7-2	B	440–520	5	0.47	0.72	5.1	2.9	9.4 ± 0.6	9.7 ± 1.2
							ND7-3	A	515–565	6	0.38	0.75	4.8	2.4	5.9 ± 0.4	
							ND7-4	B	440–610	8	0.90	0.79	21.3	8.7	11.0 ± 0.4	
							ND7-6	B	460–580	6	0.81	0.72	6.7	3.3	9.2 ± 0.8	
ND8 (nd8)	35	69	8	401	2.8	2/4	ND8-1	A	20–610	16	0.98	0.55	23.6	6.3	15.4 ± 0.4	17.4 ± 2.8
							ND8-2	A	200–580	13	0.96	0.67	11.9	3.6	20.9 ± 1.1	
ND9 (nd9)	28	67	8	389	2.8	1/3	ND9-7	B	480–580	5	0.90	0.48	11.8	6.8	18.5 ± 0.7	
ND10 (nd10)	18	69	7	281	3.6	2/3	ND10-4	A	480–580	5	0.86	0.61	9.3	5.4	13.1 ± 0.7	13.1 ± 0.03
							ND10-5	A	515–565	6	0.58	0.76	17.8	8.9	13.1 ± 0.3	
ND11 (nd11)	7	66	6	444	3.2	3/4	ND11-1	A	440–580	7	0.87	0.65	7.8	3.5	11.1 ± 0.8	13.3 ± 1.0
							ND11-3	B	460–580	6	0.87	0.55	10.0	5.0	13.2 ± 0.6	
							ND11-4	B	440–580	7	0.90	0.60	14.6	6.5	14.5 ± 0.5	
ND12 (nd12)	14	66	8	464	2.6	4/4	ND12-1	A	480–580	5	0.83	0.63	6.3	3.6	11.5 ± 1.0	13.8 ± 2.2
							ND12-2	A	480–610	6	0.92	0.73	12.4	6.2	11.3 ± 0.6	
							ND12-5	A	480–610	6	0.93	0.76	7.4	3.7	10.7 ± 1.0	
							ND12-6	B	440–580	7	0.83	0.67	13.3	5.9	19.9 ± 0.8	
ND13 (nd13)	10	69	8	191	4.0	1/3	ND13-3	B	460–580	6	0.89	0.52	4.9	2.4	6.7 ± 0.6	

Table 2 (*Continued*).

Site	Dec	Inc	N_d	k	α_{95}	n/N	Sample	Cl.	ΔT	N_p	f	g	q	w	$F_p \pm \sigma_{F_p}$	$\tilde{F}_p \pm \sigma_{\tilde{F}_p}$
ND14 (nd14)	20	65	10	94	5.1	4/4	ND14-1	A	480–580	5	0.51	0.69	7.8	4.5	5.8 ± 0.3	8.6 ± 1.9
							ND14-2	A	440–580	6	0.57	0.72	5.9	3.0	6.1 ± 0.4	
							ND14-3	B	440–550	6	0.40	0.65	2.4	1.2	5.9 ± 0.7	
							ND14-6	A	200–580	13	0.90	0.68	16.4	4.9	13.3 ± 0.5	
ND25 (nd25)	31	64	6	54	9.2	3/4	ND25-1	B	480–580	5	0.92	0.5	7.9	4.53	13.9 ± 0.9	15.9 ± 2.3
							ND25-2	A	480–580	5	0.92	0.61	8.0	4.6	11.0 ± 0.8	
							ND25-7	A	460–580	6	0.90	0.52	27.8	13.9	18.1 ± 0.3	
ND26 (nd26)	38	62	10	310	2.7	3/4	ND26-1	A	480–580	5	0.84	0.41	5.9	3.4	7.6 ± 0.4	8.4 ± 0.4
							ND26-3	A	480–580	5	0.84	0.57	9.1	5.3	8.8 ± 0.5	
							ND26-4	B	480–580	5	0.72	0.47	3.9	2.3	8.8 ± 0.8	
TK3 (tk3)	26	69	8	60	7.2	0/3										
TK4 (tk4)	23	75	8	230	3.7	2/4	TK4-1	B	200–500	10	0.45	0.76	4.0	1.4	18.2 ± 1.6	13.8 ± 3.4
							TK4-3	B	200–520	11	0.58	0.73	10.6	3.5	12.0 ± 0.5	
TK5 (tk5)	35	70	8	90	5.9	2/5	TK5-1	A	300–480	7	0.31	0.72	5.9	2.6	21.6 ± 0.8	12.9 ± 6.9
							TK5-7	B	300–520	9	0.58	0.55	13.8	5.2	8.4 ± 0.2	
TK6 (tk6)	67	75	9	143	4.3	2/4	TK6-6	B	480–580	5	0.85	0.70	9.4	5.5	9.3 ± 0.6	10.5 ± 1.1
							TK6-8	B	480–610	6	0.86	0.72	14.5	7.2	11.5 ± 0.5	
TK7 (tk7)	76	77	10	542	2.1	2/4	TK7-4	B	460–610	7	0.86	0.72	16.6	7.4	8.4 ± 0.3	9.2 ± 0.8
							TK7-7	B	460–580	6	0.86	0.70	17.2	8.6	9.9 ± 0.3	
Listvjanka section																
GD5 (gd5)	94	73	5	538	3.3	0/3										
GD4 (gd4)	82	51	5	109	7.4	1/2	GD4-7	A	300–550	10	0.57	0.75	11.1	3.9	14.3 ± 0.6	
GD3 (gd3)	114	58	7	172	4.6	2/3	GD3-2	A	480–580	5	0.81	0.58	10.1	5.8	4.3 ± 0.2	8.8 ± 4.4
							GD3-5	A	480–580	5	0.77	0.57	11.0	6.4	13.0 ± 0.5	
GD2 (gd2)	127	69	7	225	4.0	0/4										
GD1 (gd1)	145	55	8	91	5.9	2/5	GD1-5	A	100–480	10	0.40	0.80	5.2	1.8	12.8 ± 0.8	13.1 ± 0.2
							GD1-6	A	20–480	11	0.49	0.82	7.0	2.3	13.2 ± 0.8	
SV11 (sv11)	153	58	6	174	5.1	0/4										
SV10 (sv10)	151	53	6	491	3.0	1/4	SV10-5	A	480–580	5	0.79	0.56	13.5	7.8	8.6 ± 0.3	
SV9 (sv9)	161	50	4	147	7.6	3/4	SV9-1	B	410–580	8	0.26	0.73	6.7	2.7	12.8 ± 0.7	12.2 ± 1.6
							SV9-4	A	200–580	13	0.36	0.86	7.1	2.1	10.1 ± 0.4	
							SV9-6	B	250–610	13	0.29	0.86	2.6	0.8	15.3 ± 1.4	
SV8 (sv8)	155	56	6	128	5.9	4/4	SV8-1	A	410–610	9	0.31	0.67	4.2	1.6	12.4 ± 0.6	13.8 ± 1.7
							SV8-2	B	300–580	11	0.26	0.84	2.5	0.8	16.9 ± 1.5	
							SV8-4	B	250–610	13	0.33	0.90	5.1	1.6	16.4 ± 1.0	
							SV8-6	B	350–580	10	0.27	0.83	2.9	1.04	9.6 ± 0.7	
SV7 (sv7)	148	56	6	240	4.3	4/4	SV7-2	B	200–520	11	0.52	0.89	6.9	2.3	15.1 ± 1.0	14.3 ± 1.3
							SV7-3	A	200–500	10	0.51	0.88	11.0	3.9	11.0 ± 0.5	
							SV7-6	A	300–610	15	0.33	0.75	2.9	0.8	14.0 ± 1.2	
							SV7-7	B	350–500	7	0.47	0.82	8.3	3.7	17.4 ± 0.8	
SV6 (sv6)	152	54	7	116	5.6	3/3	SV6-1	B	500–610	5	0.79	0.64	11.4	6.6	4.9 ± 0.2	5.4 ± 0.6
							SV6-2	B	380–520	7	0.75	0.67	9.9	4.4	6.7 ± 0.3	
							SV6-6	B	410–550	7	0.55	0.64	8.1	3.6	4.7 ± 0.0	
SV5 (sv5)	149	54	5	448	3.7	2/3	SV5-1	B	460–610	7	0.91	0.74	10.9	4.9	5.8 ± 0.4	7.0 ± 1.6
							SV5-2	B	250–580	12	0.94	0.79	9.3	2.9	8.9 ± 0.7	
SV4 (sv4)	153	55	8	107	5.4	3/3	SV4-1	A	440–580	7	0.92	0.62	17.0	7.6	4.6 ± 0.2	5.5 ± 1.7
							SV4-2	B	440–580	7	0.90	0.53	17.0	7.6	4.7 ± 0.1	
							SV4-6	A	300–550	10	0.32	0.85	9.0	3.2	9.3 ± 0.3	
SV3 (sv3)	148	48	7	122	5.5	2/3	SV3-1	B	500–610	5	0.79	0.61	4.6	2.7	5.7 ± 0.6	7.4 ± 1.6
							SV3-3	A	480–580	5	0.33	0.65	5.3	3.1	9.0 ± 0.4	
SV2 (sv2)	148	58	5	129	6.8	2/4	SV2-1	A	200–520	11	0.53	0.88	9.4	3.1	8.6 ± 0.4	7.0 ± 1.7
							SV2-2	B	250–550	11	0.64	0.78	9.1	3.0	5.3 ± 0.3	
SV1 (sv1)	152	55	8	136	4.9	2/3	SV1-1	B	350–520	8	0.51	0.83	6.9	2.8	9.4 ± 0.6	9.8 ± 0.4
							SV1-2	B	250–550	11	0.76	0.87	8.3	2.8	10.2 ± 0.8	

Table 2 (*Continued*).

Site	Dec	Inc	N_d	k	α_{95}	n/N	Sample	Cl.	ΔT	N_p	f	g	q	w	$F_p \pm \sigma_{F_p}$	$\tilde{F}_p \pm \sigma_{\tilde{F}_p}$
IV4 (iv4)																
IV3 (iv3)	258	−70	5	318	4.4	1/4	IV3-1	B	200–440	7	0.40	0.73	2.3	1.0	9.4 ± 1.2	
IV2 (iv2)	236	−62	8	143	4.6	1/1	IV2-1	B	440–520	5	0.65	0.72	9.5	5.5	11.0 ± 0.6	
IV1 (iv1)	261	−65	6	396	3.4	0/2										
Talnakh section																
TA8 (Syver.)	146	58	8	104	5.4	0/2										
TA7	152	49	8	71	6.6	0/2										
TA6	166	56	6	25	13.8	0/2										
TA5	195	−61	4	5891	1.2	0/2										
TA4	280	−78	8	57	7.5	0/2										
TA3	236	−66	7	99	6.2	0/2										
TA1-2																

[a] The results are listed in stratigraphic order from top (KMX4) to bottom (TA1-2). In brackets are given the site identification as used in [21]. The Talnakh profile is parallel to the lower part of the Listvjanka section. Dec and Inc denote declination and inclination, respectively, N_d the number of samples used to calculate the mean flow direction. n/N denotes the ratio of successful to performed Thellier experiments, Cl. the quality class according to the reliability criteria (see text). ΔT specifies the temperature range of the linear segment in the NRM–TRM plots, N_p the number of successive data points used for the calculation of the palaeointensity. f, g and q are the fraction of the NRM, the gap and quality factor as defined by Coe et al. [37], respectively. $F_p \pm \sigma_{F_p}$ represents the result of an individual palaeointensity experiment and its associated standard deviation. $\tilde{F}_p \pm \sigma_{\tilde{F}_p}$ is, if applicable, the calculated weighted mean palaeointensity using the weighting factor w of Prévot et al. [9].

slightly deviant to the stable reversed pole. Table 1 summarises the directions and pole positions of the groups as defined above.

Compared to today's strength of the EMF significantly lower VDM values are observed throughout the record. Unfortunately, the section comprises only a few flows of reversed polarity. No reliable mean palaeointensity of the reversed polarity interval could be obtained from the studied section. But there seems to be a trend to slightly decreased intensities during the clustering of transitional directions (group B, 12 flows of the Listvjanka and three flows of the Talnakh section) which is followed by a remarkable increase to twice the values (from around 6 to 13 μT). The clustering may be explained by an episode of rapid succession of lava flows [41–43]. The palaeointensity results, however, indicate that this phenomenon has a geomagnetic cause as several independent field states were recorded. Two alternatives can account for this observation: (1) Assuming a mainly non-dipolar transitional field configuration, a strong local magnetic flux, also resulting in relatively constant local field directions, must build up to explain the increase in intensity [2]. (2) Hoffman [10,11] suggested that during a transition the field has quasi-stable configurations in which dipolar components are relatively strong. The inherent instability of a geodynamo fluid pattern where the axis of the magnetic field and the rotational axis are far apart causes this dipolar configuration to decay. The following non-dipolar configuration provokes rapid directional changes until a new quasi-stable state or a stable polarity is reached. Such significant changes of the field directions are observed in the present record. Although the observed pattern can be explained by alternating phases of lulls and boosts of the volcanic activity, the data at hands show rather good agreement to Hoffman's scenario described above. It has to be admitted, however, that a definite answer cannot be given at this time.

No clear systematic palaeointensity variations are observed during or after the excursion. Palaeointensities are generally higher than during the transition. In order to get a reliable palaeointensity estimate for the Late Permian/Early Triassic we excluded palaeointensities of transitional or excursional directions. As stable normal polarity we interpret all flows above flow ND6. The calculated mean palaeointensity for this part of the section is 19.3 μT with a standard deviation of 7.2 μT. This corresponds to a mean VDM of 2.2×10^{22} Am^2 which is significantly lower than

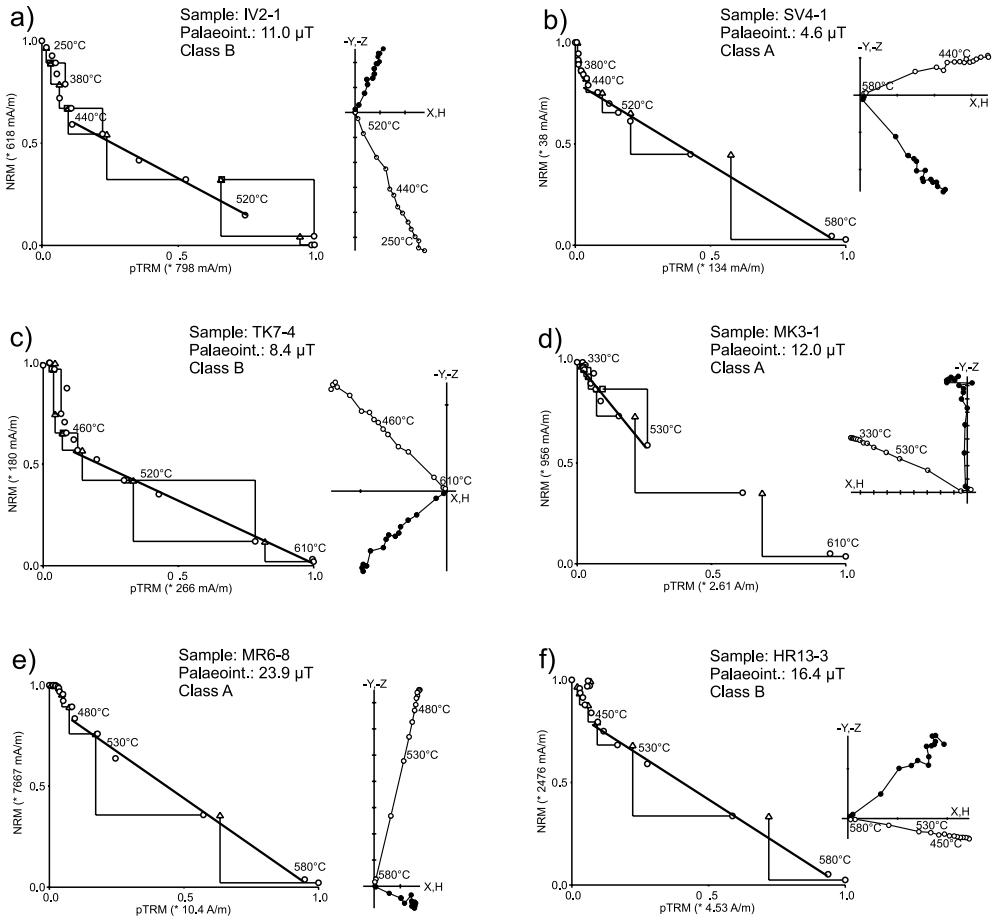

Fig. 5. Examples of successful palaeointensity determinations of the different suites.

the value of 3.4×10^{22} Am^2 obtained by Solodovnikov [44] on trap basalt samples from Noril'sk and the Lake Lama region (Thellier–Thellier without pTRM checks). However, the stratigraphic position of the samples used in that study is unclear. Both results confirm the existence of the MDL and define up to now its lower boundary. More data constraining the extension of the MDL in the geological past are needed, though.

In order to estimate the palaeosecular variation, the VGP dispersion [45] for the stable normal part of the section (group D, containing no major time gaps) and the associated cut-off angle A was calculated. This procedure yielded an $A = 32°$. No results had to be disregarded using this iterative method. The data were corrected for the within-site scatter [46]. This correction is a function of the latitude which was in our case defined as the palaeolatitude obtained from the mean pole of group D assuming a geocentric axial dipole. The VGP dispersion (S_F) yielded a value of 15.4° with upper and lower 95% confidence limits [47] of $S_u = 18.1°$ and $S_l = 13.4°$, respectively. Compared to analyses of the palaeosecular variation of the last 5 Ma, which yields $S_F = 20.3°$ [46] for the respective latitude, this value is clearly lower. However, it has to be noted that this discrepancy is caused by the larger cut-off angle (42.6°) used in that study. A query of the palaeosecular variation RL database, designed by McElhinny and Lock [48] and currently maintained by S. Pisarevsky, using a cut-off angle of 30° (0–5 Ma, 104 data

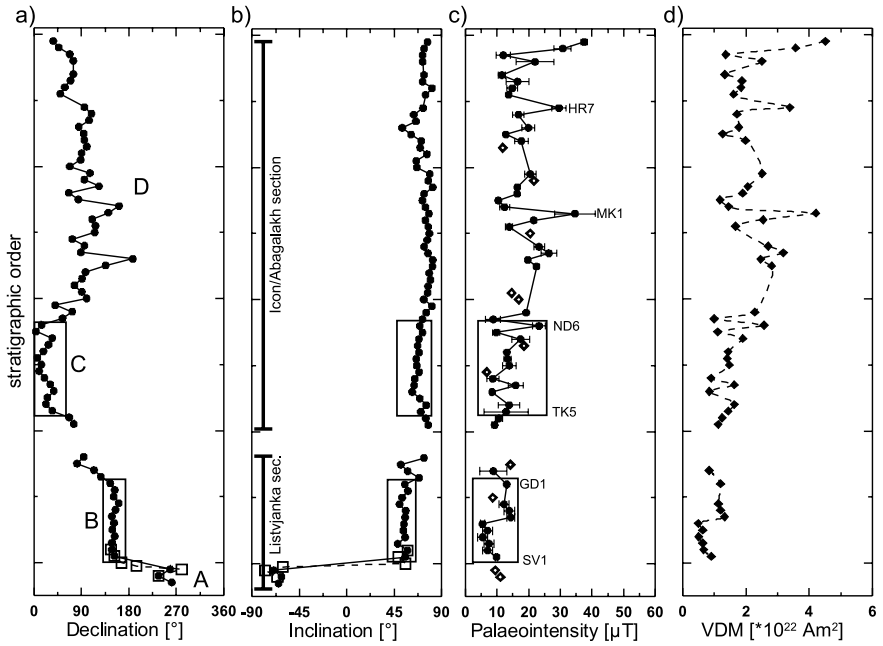

Fig. 6. Declination (a), inclination (b), palaeointensity (c) and VDM (d) across the studied sections. The results of the Talnakh section are indicated by open squares and a broken line. Open symbols in (c) denote results of lava flows with only one successful Thellier–Thellier determination. The gap between the Listvjanka and the Abagalakh sections comprises only the Khakanchansky suite, which has in the Noril'sk area a thickness of 10–130 m (mainly tuffs). Outcrops of this suite were not found in the studied areas. However, borehole data [21] prove that this suite is also of normal polarity. Also given are the directional clusters (A–D) and the position of individual flows for orientation.

sets) yields a S_F of 17° ($S_u = 18.9°$, $S_l = 15.5°$). Thus, our results indicate that the palaeosecular variation in the earliest Triassic was somewhat but not significantly lower. Results of Lyons et al. [49] obtained from 15 cooling units of the Early Triassic Semeitau igneous series (Kazakhstan, 248.2 Ma), likely to be genetically related to the Siberian traps, show to be at the 95% confidence level indistinguishable from the secular variation averaged over the past 5 Ma. Moreover, our results do not show an inverse correlation between angular secular variation and intensity of EMF as proposed by Love [50] for younger episodes of Earth's history. For comparison the VGP dispersion was also calculated for the transitional cluster (group B: $S_F = 4.4°$, $S_u = 5.9°$, $S_l = 3.4°$) and the post-transitional excursion (group C: $S_F = 8.1°$, $S_u = 10.8°$, $S_l = 6.4°$). But these values have to be considered with caution due to the lack of information about the time interval covered by these flows.

5. Conclusions

The palaeomagnetic record shows a reversed polarity in the Ivakinsky suite. Then, a stable transitional pole is recorded in the Syverminsky suite followed by a motion of the VGPs towards the position of the mean pole of the Abagalakh section. The record of the Icon section shows a movement of the VGPs from approximately this position more or less on the same latitude eastwards and back again which is tentatively interpreted as an excursion. The palaeointensity record displays high variability with values ranging from around 10 to 40 μT and has a minimum around 6 μT during the transition. A striking feature of the directional cluster of the transitional field is a doubling in palaeointensity values during this period. The preferred interpretation of this feature is that this cluster is not an artefact caused by high extrusion rates, but is rather indicative for a considerable directional stability of the transitional

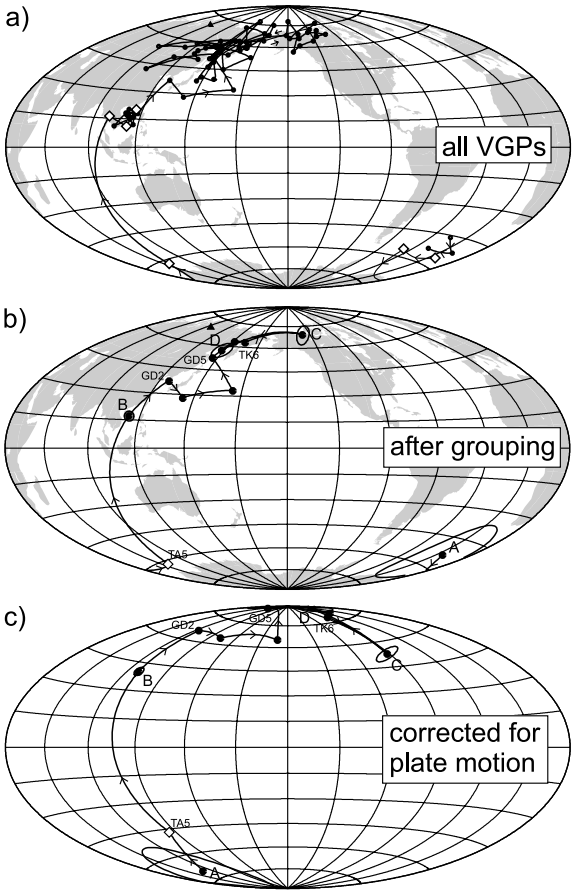

Fig. 7. Movement of the VGPs across the studied sections (Hammer projection, centred at the 210° meridian). The site location is denoted by a triangle. (a) all VGPs, the results of the Talnakh profile, parallel to the bottom of the Listvjanka section, are denoted by open diamonds. (b) Shown as black dots are the groups as defined in the text with their associated d_m and d_p confidence limits and the VGPs of individual flows not belonging to one of the groups. The lowest part is characterised by reversed polarities (group A and two flows of the Talnakh section) and then reaches a stable transitional cluster (Group B, 15 flows). The following four flows (GD2–GD5) move towards normal polarity. The first flows (TK7 and TK6) of the Icon/Abagalakh section have directions typical for Early Triassic normal polarity, but then an excursion to more easterly pole positions is observed (group C, 14 flows) before reaching again the normal pole (group D). (c) The same VGPs as in (b) after correction for Permo-Triassic palaeogeography. Continents in (a) and (b) are plotted in their present positions.

field. This clustering, low intensities during the transitional field configuration and the excursion shortly after the reversal are patterns observed in several younger reversals [9–13] and suggest that the underlying reversal processes in the Early Triassic were basically the same. The mean VDM for the period of stable normal polarity is calculated and yields a distinctly lower VDM ($2.2 \pm 0.9 \times 10^{22}$ Am^2) compared to the present-day EMF confirming that the Mesozoic dipole extends at least down to the Late Permian/Early Triassic. Taking into account the results of the palaeosecular variation estimates which yield comparable values to those for the last 5 Ma, a direct link between intensity and secular variation seems unlikely.

Acknowledgements

This work was supported by the Priority Program 'Geomagnetic Variations' of the Deutsche Forschungsgemeinschaft, grants So72/66-1 (C.H.) and Pe173/12-1 (D.K.). We gratefully acknowledge the help of V. Vodovozov and V. Rad'ko during field work. Roman Leonhardt provided the analytical software and we appreciated his valuable suggestions. We also thank Jean-Pierre Valet, Rob Coe, an anonymous reviewer and the editor Vincent Courtillot for their helpful comments that improved the manuscript. Thanks to the Munich gang.*[VC]*

References

[1] G.A. Glatzmaier, R.S. Coe, L. Hongre, P.H. Roberts, The role of the earth's mantle in controlling the frequency of geomagnetic reversals, Nature 401 (1999) 885–890.
[2] R.S. Coe, L. Hongre, G.A. Glatzmaier, An examination of simulated geomagnetic reversals from a paleomagnetic perspective, Philos. Trans. R. Soc. London 357 (2000) 1787–1813.
[3] R.T. Merrill, P.L. McFadden, Geomagnetic polarity transitions, Rev. Geophys. 37 (1999) 201–226.
[4] V. Shcherbakov, G.M. Solodovnikov, N.K. Sycheva, Variations in the geomagnetic dipole during the past 400 million years (volcanic rocks), Izv. Acad. Sci. Phys. Solid Earth 38 (2002) 113–119.
[5] A.S. Bol'shakov, G.M. Solodovnikov, Geomagnetic field

intensity in Armenia in the Late Jurassic and Early Cretaceous, Izv. Acad. Sci. Phys. Solid Earth 19 (1983) 976–982.
[6] M. Prévot, M. El-Messaoud Derder, M. McWilliams, J. Thompson, Intensity of the Earth's magnetic field: Evidence for a Mesozoic dipole low, Earth Planet. Sci. Lett. 97 (1990) 129–139.
[7] H. Tanaka, M. Kono, H. Uchimura, Some global features of paleointensity in geological time, Geophys. J. Int. 120 (1995) 97–102.
[8] M. Perrin, V. Shcherbakov, Paleointensity of the Earth's magnetic field for the past 400 Ma: Evidence for a dipole structure during the Mesozoic low, J. Geomagn. Geoelectr. 49 (1997) 601–614.
[9] M. Prévot, E.A. Mankinen, R.S. Coe, C.S. Grommé, The Steens Mountain (Oregon) geomagnetic polarity transition 2. Field intensity variations and discussion of reversal models, J. Geophys. Res. 90 (1985) 10417–10448.
[10] K.A. Hoffman, Dipolar reversal state of the geomagnetic field and core-mantle dynamics, Nature 359 (1992) 789–794.
[11] K.A. Hoffman, Transitional paleomagnetic field behavior: Preferred paths or patches, Surv. Geophys. 17 (1996) 207–211.
[12] R. Leonhardt, J. Matzka, F. Hufenbecher, H.C. Soffel, F. Heider, A reversal of the Earth's magnetic field recorded in Mid-Miocene lava flows of Gran Canaria: Paleodirections, J. Geophys. Res. 107 (2002) EPM5-1–EPM5-11.
[13] J. Riisager, P. Riisager, A.K. Pedersen, The C27n-C26r geomagnetic polarity reversal recorded in the West Greenland flood basalt province: How complex is the transitional field?, J. Geophys. Res. 108 (2002) EPM4-1–EPM4-11.
[14] E. Thellier, O. Thellier, Sur l'intensité du champ magnétique terrestre dans le passé historique et géologique, Ann. Géophys. 15 (1959) 285–376.
[15] R.S. Coe, The determination of paleointensities of the Earth's magnetic field with emphasis on mechanisms which could cause non-ideal behavior in Thelliers method, J. Geomagn. Geoelectr. 19 (1967) 157–179.
[16] E. McClelland, J.C. Briden, An improved methodology for Thellier-type paleointensity determination in igneous rocks and its usefulness for verifying primary thermoremanence, J. Geophys. Res. 101 (1996) 21995–22013.
[17] J.P. Valet, J. Brassart, I. LeMeur, V. Soler, X. Quidelleur, E. Tric, P.Y. Gillot, Absolute paleointensity and magnetomineralogical changes, J. Geophys. Res. 101 (1996) 25029–25044.
[18] R. Leonhardt, F. Hufenbecher, F. Heider, H.C. Soffel, High absolute paleointensity during a Mid-Miocene excursion of the Earth's magnetic field, Earth Planet. Sci. Lett. 184 (2000) 141–154.
[19] P. Riisager, J. Riisager, Detecting multidomain magnetic grains in thellier palaeointensity experiments, Phys. Earth Planet. Int. 125 (2001) 111–117.
[20] D. Krása, C. Heunemann, R. Leonhardt, N. Petersen, Experimental procedure to detect multidomain remanence during Thellier–Thellier experiments, Phys. Chem. Earth 28 (2003) 681–687.
[21] E. Gurevitch, C. Heunemann, V. Rad'ko, M. Westphal, V. Bachtadse, J.P. Pozzi, H. Feinberg, Palaeomagnetism and magnetostratigraphy of the Permian–Triassic Siberian trap basalts, Tectonophysics (doi:10.1016/S0040-1951(03)0005377), in press.
[22] V.A. Fedorenko, P.C. Lightfoot, A.J. Naldrett, G.K. Czamanske, C.J. Hawkesworth, J.L. Wooden, D.S. Ebel, Petrogenesis of the flood-basalt sequence at Noril'sk, North Central Siberia, Int. Geol. Rev. 38 (1996) 99–135.
[23] M.K. Reichow, A.D. Saunders, R.V. White, M.S. Pringle, A.I. Al'Mukhamedov, A.I. Medvedev, N.P. Kirda, Ar-40/Ar-39 dates from the West Siberian Basin: Siberian flood basalt province doubled, Science 296 (2002) 1846–1849.
[24] S.L. Kamo, G.K. Czamanske, T.E. Krogh, A minimum U–Pb age for Siberian Flood-Basalt volcanism, Geochim. Cosmochim. Acta 60 (1996) 3505–3511.
[25] P.R. Renne, Z.C. Zhang, M.A. Richards, M.T. Black, A.R. Basu, Synchrony and causal relations between Permian–Triassic boundary crises and Siberian flood volcanism, Science 269 (1995) 1413–1416.
[26] P.R. Renne, A.R. Basu, Rapid eruption of the Siberian Traps Flood Basalts at the Permo-Triassic boundary, Science 253 (1991) 176–179.
[27] P.B. Wignall, Large igneous provinces and mass extinctions, Earth Sci. Rev. 53 (2001) 1–33.
[28] V. Courtillot, P.R. Renne, On the ages of flood basalt events, C. R. Geosci. 335 (2003) 113–140.
[29] V. Courtillot, C. Jaupart, I. Manighetti, P. Tapponnier, J. Besse, On causal links between flood basalts and continental breakup, Earth Planet. Sci. Lett. 166 (1999) 177–195.
[30] A.M. Nikishin, P.A. Ziegler, D. Abbott, M.F. Brunet, S. Cloetingh, Permo-Triassic intraplate magmatism and rifting in Eurasia: implications for mantle plumes and mantle dynamics, Tectonophysics 351 (2002) 3–39.
[31] M. Sharma, Siberian traps, in: J.J. Mahoney, M.F. Coffin (Eds.), Large Igneous Provinces: Continental, Oceanic, and Planetary Flood Volcanism, Geophysical Monograph Series, Vol. 100, American Geophysical Union, 1997, pp. 273–295.
[32] E.N. Lind, S.V. Kropotov, G.K. Czamanske, C.S. Grommé, V.A. Fedorenko, Paleomagnetism of the Siberian flood basalts of the Noril'sk area: A constraint on eruption duration, Int. Geol. Rev. 36 (1994) 1139–1150.
[33] D.J. Dunlop, Ö. Özdemir, Rock Magnetism: Fundamentals and Frontiers, Cambridge Studies in Magnetism, Cambridge University Press, Cambridge, 1997.
[34] J. Matzka, D. Krása, T. Kunzmann, A. Schult, N. Petersen, Magnetic state of 10 to 40 Ma old ocean basalts and its implications for natural remanent magnetization, Earth Planet. Sci. Lett. 206 (2002) 541–553.
[35] Y. Arai, Secular variation in intensity of the Past Geomagnetic Field, Msc Thesis, University of Tokyo, Japan, 1963.

[36] J.D.A. Zijderveld, Demagnetization: Analysis of results, Methods of Paleomagnetism, Elsevier, Amsterdam, 1967.
[37] R.S. Coe, C.S. Grommé, E.A. Mankinen, Geomagnetic paleointensities from radiocarbon-dated lava flows on Hawaii and the question of the Pacific Nondipole Low, J. Geophys. Res. 83 (1978) 1740–1756.
[38] R.T. Merrill, M.W. McElhinny, P.L. McFadden, The Magnetic Field of the Earth, Academic Press, San Diego, CA, 1998.
[39] M.A. Smethurst, A.N. Khramov, T.H. Torsvik, The Neoproterozoic and Palaeozoic palaeomagnetic data for the Siberian platform: From Rodinia to Pangea, Earth Sci. Rev. 43 (1998) 1–24.
[40] P. McFadden, M. McElhinny, Classification of the reversal test in palaeomagnetism, Geophys. J. Int. 103 (1990) 725–729.
[41] J.J. Love, Paleomagnetic volcanic data and geometric regularity of reversals and excursions, J. Geophys. Res. 103 (1998) 12435–12452.
[42] E. Herrero-Bervera, J.P. Valet, Paleosecular variation during sequential geomagnetic reversals from Hawaii, Earth Planet. Sci. Lett. 171 (1999) 139–148.
[43] J.P. Valet, E. Herrero-Bervera, Some characteristics of geomagnetic reversals inferred from detailed volcanic records, C. R. Geosci. 335 (2003) 79–90.
[44] G.M. Solodovnikov, Palaeointensity of the Early Triassic geomagnetic field, Izv. Acad. Sci. Phys. Solid Earth 30 (1995) 815–821.
[45] D. Vandamme, A new method to determine paleosecular variation, Phys. Earth Planet. Int. 85 (1994) 131–142.
[46] M.W. McElhinny, P.L. McFadden, Palaeosecular variation over the past 5 Myr based on a new generalized database, Geophys. J. Int. 131 (1997) 240–252.
[47] A. Cox, Confidence limits for the precision parameter k, Geophys. J. R. Astron. Soc. 18 (1960) 545–549.
[48] M.W. McElhinny, J. Lock, IAGA palaeomagnetic databases with Access, Surv. Geophys. 17 (1996) 575–591.
[49] J.J. Lyons, R.S. Coe, X.X. Zhao, P.R. Renne, A.Y. Kazansky, A.E. Izokh, L.V. Kungurtsev, D.V. Mitrokhin, Paleomagnetism of the Early Triassic Semeitau igneous series, eastern Kazakstan, J. Geophys. Res. 107 (2002) EPM4-1–EPM4-15.
[50] J.J. Love, Palaeomagnetic secular variation as a function of intensity, Philos. Trans. R. Soc. London Ser. A Math. Phys. Eng. Sci. 358 (2000) 1191–1223.